Intrinsic position uncertainty explains detection and localization performance in peripheral vision

Melchi Michel

Center for Perceptual Systems, University of Texas at Austin, Austin, USA, & Department of Psychology, University of Texas at Austin, Austin, USA

Wilson S. Geisler

Center for Perceptual Systems, University of Texas at Austin, Austin, USA, & Department of Psychology, University of Texas at Austin, Austin, USA

Efficient performance in visual detection tasks requires excluding signals from irrelevant spatial locations. Indeed, researchers have found that detection performance in many tasks involving multiple potential target locations can be explained by the uncertainty the added locations contribute to the task. A similar type of Location Uncertainty may arise within the visual system itself. Converging evidence from hyperacuity and crowding studies suggests that feature localization declines rapidly in peripheral vision. This decline should add inherent position uncertainty to detection tasks. The current study used a modified detection task to measure how intrinsic position uncertainty changes with eccentricity. Subjects judged whether a Gabor target appeared within a cued region of a noisy display. The eccentricity and size of the region varied across blocks. When subjects detected the target, they used a mouse to indicate its location. This allowed measurement of localization as well as detection errors. An ideal observer degraded with internal response noise and position noise (uncertainty) accounted for both the detection and localization performance of the subjects. The results suggest that position uncertainty grows linearly with visual eccentricity and is independent of target contrast. Intrinsic position uncertainty appears to be a critical factor limiting search and detection performance.

Keywords: detection/discrimination, spatial vision, computational modeling, attention, search

Citation: Michel, M., & Geisler, W. S. (2011). Intrinsic position uncertainty explains detection and localization performance in peripheral vision. *Journal of Vision, 11*(1):18, 1–18, http://www.journalofvision.org/content/11/1/18, doi:10.1167/11.1.18.

Introduction

Natural tasks involving the detection of visual targets typically include considerable uncertainty about the location and form of the target. For example, a radiologist examining an X-ray or MRI image for evidence of a tumor must consider many possible tumor locations and configurations. Researchers have long realized that such uncertainty can reduce detection performance (e.g., Cohn & Lasley, 1974; Pelli, 1985; Peterson, Birdsall, & Fox, 1954; Tanner, 1961). Any uncertainty in the identity, timing, or position of a target requires the observer to consider irrelevant features (e.g., stimuli from irrelevant time intervals or irrelevant spatial locations) and results in reduced detection performance compared with an ideal observer without such uncertainty (Pelli, 1985; Peterson et al., 1954). Thus, a central part of any visual detection task consists of isolating the relevant aspects of the stimulus array. The radiologist in the example above, for example, is more likely to successfully detect a tumor if it has a stereotypical morphology and if she knows where in the image the tumor is likely to appear. Knowledge of spatial location or position is especially important when an observer must detect small targets in a background of clutter having similar features. Almost everyone has experienced the effect of this position uncertainty in the form of a lost cursor. Though small, computer cursors are typically easy to detect in isolation and even in clutter, if we know roughly where to find them. However, when we lose track of a cursor's position, it can be difficult to detect because we must now consider hundreds or even thousands of nonoverlapping positions for the cursor. This position uncertainty can reduce the detectability of the target by more than an order of magnitude (Cohn & Wardlaw, 1985).

Position uncertainty can arise in two ways: *extrinsic* and *intrinsic*. Extrinsic position uncertainty occurs when the location of the signal is randomly sampled from a set of potential locations or is otherwise imprecisely specified within the task. Experiments that directly manipulate extrinsic position uncertainty are sometimes called *uncertainty* experiments (e.g., Cohn & Lasley, 1974; Pelli, 1985) and sometimes single-fixation *visual search* experiments

doi: 10.1167/11.1.18 Received August 17, 2010; published January 21, 2011 ISSN 1534-7362

(e.g., Cameron, Tai, Eckstein, & Carrasco, 2004; Eckstein, 1998; Palmer, 1994; Palmer, Verghese, & Pavel, 2000).

Measuring the effects of extrinsic position uncertainty on detection requires taking into account the effects of retinal eccentricity because the resolution of the human visual system drops rapidly away from the point of gaze. When eccentricity effects are controlled, researchers have found that performance in a variety of detection and discrimination tasks involving multiple potential target locations is explained largely by the uncertainty that the added locations contribute to the task (e.g., Baldassi & Burr, 2000; Burgess & Ghandeharian, 1984; Cameron et al., 2004; Cohn & Wardlaw, 1985; Cohn & Lasley, 1974; Eckstein & Whiting, 1996; Eckstein, 1998; Eckstein, Thomas, Palmer, & Shimozaki, 2000; Palmer, 1994; Palmer, Ames, & Lindsey, 1993; Shaw, 1982; Swensson & Judy, 1981).

In an analogous manner, intrinsic position uncertainty can arise within the visual system itself when the observer is unable to precisely localize or isolate the spatial source of a stimulus. Tanner (1961) first observed that human psychometric functions in a signal-known-exactly (SKE) detection task can match the shape of the psychometric functions of an ideal observer in an extrinsic uncertainty task where one of many signals could appear. Tanner, and later Pelli (1985), suggested that models of human detection performance might be wrong in assuming exact knowledge of the signal in such tasks, because humans may in fact be unable to precisely represent the signal or exploit such a representation in the detection task. Moreover, they suggested that one might be able to characterize a human observer's effective intrinsic uncertainty by comparing human performance to that of an ideal observer under varying conditions of extrinsic uncertainty. In a detection task, adding intrinsic position uncertainty reduces performance in much the same way as adding potential target locations. In this case, even when the spatial location of the target is specified exactly by the experimenter (an SKE task) the observer must integrate across irrelevant adjacent locations, because the representation of location is noisy.

Evidence from position discrimination (e.g., Hess & Hayes, 1994; Levi & Tripathy, 1996; Westheimer, 1982) and crowding (e.g., Bouma, 1970; Levi, 2008; Pelli, Palomares, & Majaj, 2004) studies shows that the ability to spatially localize or isolate features declines in peripheral vision at a rate greater than that predicted by the falloff in spatial resolution. These studies suggest that intrinsic position uncertainty increases with eccentricity. On the other hand, many studies that varied extrinsic position uncertainty in the periphery found that performance closely matches the predictions of the ideal observer with no intrinsic uncertainty. However, these studies minimized the effects of intrinsic position uncertainty in the periphery either by using well-separated spatial locations (Cohn & Lasley, 1974; Eckstein, 1998; Eckstein et al., 2000), by allowing unrestricted eye movements (Bochud, Abbey, & Eckstein, 2004; Burgess & Ghandeharian, 1984; Eckstein & Whiting, 1996; Swensson & Judy, 1981), or by limiting the region of uncertainty to locations within the fovea (Cohn & Wardlaw, 1985). On the other hand, studies that varied extrinsic uncertainty using contiguous extrinsic uncertainty regions found that performance deviated from the predictions of the extrinsic uncertainty ideal observer (Pelli, 1981, Appendix 6; Shiffrin, McKay, & Shaffer, 1976). This is not unexpected because under these circumstances intrinsic uncertainty can mask the effects of extrinsic uncertainty.

As a simple example of the relationship between extrinsic and intrinsic uncertainties, consider a task in which an observer briefly views a display composed of two noisy patches and is asked to report whether a target was present within the display. Assume that we can model the observer's internal representation of the stimulus as a pair of noisy feature responses. We can now compare two conditions for this task. In the *certain* condition, the observer is told in advance that the target, if present, will always appear within the leftmost patch. In the *uncertain* condition, the target can appear in either (but not both) of the noise patches. Because the observer can rule out one of the locations in the first condition, we should expect to see better performance in this condition compared with the second condition. More generally, as we increase the number of noise patches and locations in which the target can appear, the observer's performance will tend to decrease because the observer is forced to consider an increasing number of noisy feature responses. However, imagine that the two patches in our sample task are spatially adjacent and that the observer now has intrinsic position uncertainty such that he cannot discern whether a particular feature response came from the first or the second display location. In this case, his uncertainty about the provenance of the responses requires that he consider both responses regardless of the condition. That is, if the observer has intrinsic uncertainty that confuses the spatial sources of the signals, then we should not expect any difference in performance between the certain and uncertain conditions. More generally, intrinsic uncertainty will reduce the effect of added extrinsic uncertainty.

In the current study, we exploited this insight to determine how the effective intrinsic position uncertainty of human observers performing a detection task changes as a function of retinal eccentricity. Specifically, we evaluated the performance of human observers for both detecting and localizing (pointing to the location of) a small, briefly presented Gabor patch as a function of target contrast, retinal eccentricity, and level of extrinsic position uncertainty. We then constructed an ideal observer with detection performance that matched that of the human observers in the no extrinsic uncertainty task, where the ideal observer's intrinsic position uncertainty was set to match the human observers' asymptotic

localization (pointing) variability, which is approached at high target contrasts. We find that this ideal observer model with intrinsic position uncertainty accounts for the detection performance of the human observers in conditions where the signal is specified exactly and makes accurate parameter-free predictions of detection and localization performance under extrinsic position uncertainty conditions in which the location of the target is randomized. Our results suggest that the intrinsic position uncertainty in normal peripheral vision grows linearly with eccentricity and is independent of signal strength.

Methods

Observers

Data were collected from three human observers. All three were experienced observers who had previous experience with similar detection tasks. One of the observers was an author; the other two were naïve to the aims of the experiment. All observers had normal or corrected-to-normal acuity.

Stimuli and apparatus

The stimuli were 8-bit images displayed on a calibrated monochrome Image Systems monitor (M2IL) with white phosphor (P-104) at a frame rate of 60 Hz. The monitor was set to a resolution of 800 × 600 pixels and located 1 m from the observer so that the display subtended 15.8 × 21.1 degrees of visual angle. To provide fine control over target contrast, we combined the 24-bit RGB output signals from the graphics card to drive the electron gun voltage (Pelli & Zhang, 1991). To ensure that observers maintained fixation during the stimulus interval, eye position was measured using a Fourward-Technologies SRI Mark VI dual Purkinje eye tracker. Head position was maintained using a bite bar and headrest, and eye position signals were sampled from the eye tracker at 500 Hz. An 18-point calibration routine was used to establish a transformation between the output voltages of the eye tracker and the position of the observer's gaze on the computer display. If an eye movement was detected during the stimulus interval, the observer was notified of the break in fixation and the trial was discarded.

The target stimuli (Figure 1A) were 1-octave, 6 cycle per degree raised-cosine Gabor patterns in sine phase tilted 45° counterclockwise from the horizontal orientation. The background was a circular region 15.8 degrees (600 pixels) in diameter filled with broadband noise whose amplitude spectrum fell with frequency (i.e., $1/f$ noise). The area surrounding the circular region was set to the mean luminance of 20 cd/m^2. The $1/f$ noise was created by filtering Gaussian white noise, truncating the waveform at ±2 *SD*, scaling to obtain the desired root-mean-square (rms) amplitude and then adding a constant to obtain the mean luminance. The rms contrast of the noise region was fixed at 10% across all trials.

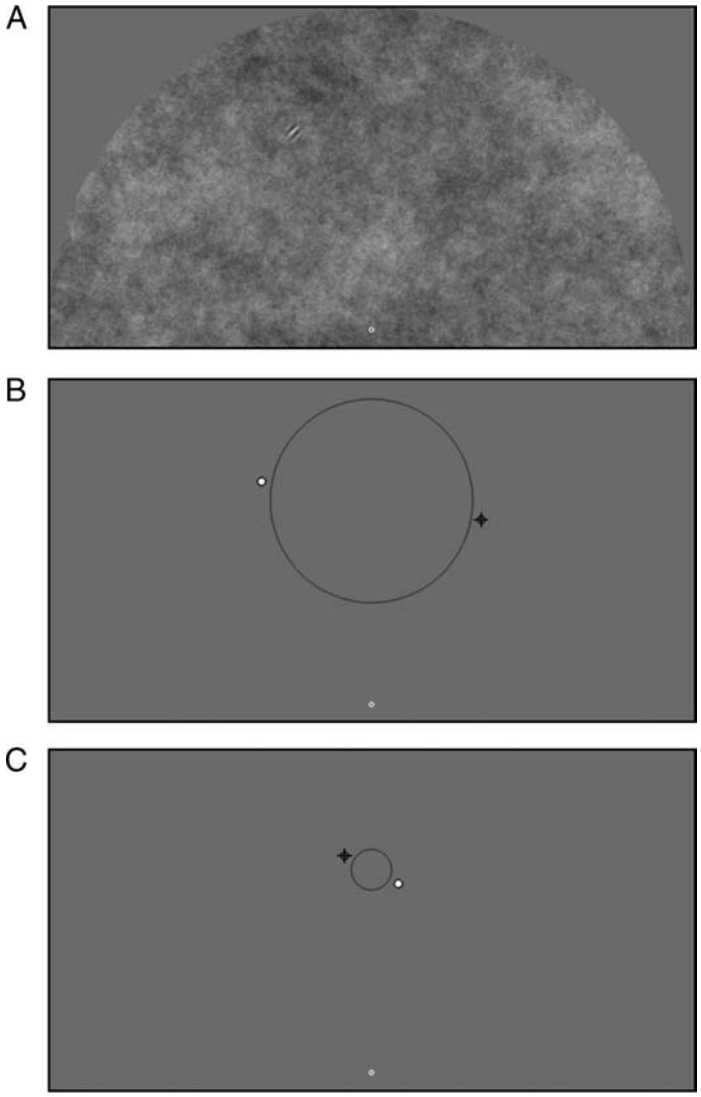

Figure 1. Detection/localization stimulus and response displays. All figures show the top half of the display for a cue eccentricity of 5.0 degrees. (A) A stimulus from the Location-Uncertain condition. The Gabor target is in the upper left part of the display. (B) The response screen for the Location-Uncertain condition. The target could appear anywhere within the cued region marked by the large black circle. (C) The response screen for the Location-Specified condition. The target always appeared in the center of the cued region. Subjects responded by positioning the black crosshairs at the remembered target location or, if no target was detected, over the filled white circle opposite the crosshairs. The small open circle at the bottom of each display is the fixation marker.

Procedure

At the start of each trial, observers fixated a small marker in the center of the display while an open circle indicated the target region. After the observer pressed a start button and after a random stimulus onset asynchrony (100–500 ms), the cue disappeared and the stimulus appeared for 250 ms. The stimulus consisted either of background noise only or of background noise with a target added within the cued region. The observer's primary task was to determine whether or not a target appeared within the target region during the stimulus interval. We refer to this task as the "detection" task. This task was augmented with a secondary task, in which the observer had to indicate where the target, if present, was located. We refer to this second task as the "localization" task.

To allow observers to perform both tasks concurrently, we had them respond using a mouse pointer. Following the stimulus interval, the response display was presented. In the response display, the open circle representing the target region reappeared along with a pointer (crosshairs in Figures 1B and 1C) and a "no target" marker. If a target was detected, the observer responded by moving the pointer to and clicking on the remembered location of the target; otherwise, the observer responded "no target" by moving the pointer to and clicking on the "no target" marker (small white circle in Figures 1B and 1C). The pointer was initialized at a random position 0.5 degree outside of the target region and "no target" marker always appeared opposite the initial position of the pointer. Responses were self-paced, without a time limit, and observers were free to make saccades to the remembered location. The "no target" marker had a radius of 0.1 degree and to qualify as a valid response, the pointer had to be positioned either within the "no target" marker or within the target region. If the observer positioned the pointer and clicked anywhere else (i.e., in an invalid region of the display), an auditory tone indicated an error and the observer was allowed to reposition the pointer. Observers rarely made such errors following their initial training and familiarization with the task.

Observers participated in two different cue conditions. In the *Location-Uncertain* (LU) condition, the target appeared at a random location within the cued region; however, to keep any part of the target from appearing outside of the cued target region, the target center was not allowed to fall within 0.3 degree of the edge of the cued region. The size of the target region for the LU condition changed with eccentricity such that the diameter of the cued region was equal to the eccentricity of the region center (e.g., a target region centered at 5° was bounded by a circle whose diameter was 5°). In the *Location-Specified* (LS) condition, the target (when present) always appeared in the center of the cued region that was 0.8° in diameter. Observers were tested at 5 different eccentricities along the upper vertical meridian (ε = {0.0°, 1.5°, 2.5°, 3.5°, 5.0°}), over a variety of target contrasts, and the trials were blocked by cue condition, target region eccentricity, and target contrast.

Intrinsic uncertainty observer

For detection of a known target in Gaussian noise, the ideal detection mechanism consists of template matching—multiplying the image with a prewhitened matched filter of the target, integrating across the image, and comparing the scalar result to a criterion (Myers, Barrett, Borgstrom, Patton, & Seeley, 1985). However, when compared with the performance of such a mechanism, human detection generally falls well short of optimal (e.g., Burgess, Wagner, Jennings, & Barlow, 1981; Lu & Dosher, 1999; Myers et al., 1985; Pelli, 1981; Tanner, 1961). This is because, in addition to the physical noise in the stimulus, human detection performance is degraded by effects of intrinsic signal uncertainty, optical aberrations, retinal sampling errors, neural noise, and other inefficiencies intrinsic to the human observer. A common and useful way to characterize these inefficiencies at a system level is to model the human perceptual system as an otherwise ideal mechanism with a separate, internal source of noise and to calculate or measure the amount of this internal noise required to degrade the performance of the ideal mechanism to match that of the human observer. The resulting measure, called equivalent internal noise (Ahumada & Watson, 1985; Lu & Dosher, 1999) or intrinsic noise (Burgess et al., 1981; Pelli, 1985), can be used to characterize changes in efficiency across task parameters. This type of characterization generally does not distinguish between various sources for the inefficiency but rather lumps together various intrinsic noise sources (Lu & Dosher, 1999; Pelli, 1985). However, different sources of intrinsic uncertainty, when incorporated into a constrained ideal observer, often predict different patterns of behavior for the same task. Through careful experiment design, it is possible to tease apart different sources of intrinsic noise (Tanner, 1961). In the current study, we model two types of intrinsic noise: *intrinsic position uncertainty* reflects factors intrinsic to the observer that contribute to uncertainty in the spatial source of the template or feature response associated with an image patch, while *intrinsic response uncertainty* reflects factors intrinsic to the observer that contribute to uncertainty in the magnitude of the response.

We compared human detection and localization performance with that of a constrained ideal observer model: the *intrinsic uncertainty observer*. To determine the performance of the intrinsic uncertainty observer, we derived the optimal detection and localization strategies for a task in which a known target is located randomly within a cued region in a field of random spatial noise. Figure 2 illustrates the important aspects of the model. In each trial, the observer attempts to determine whether or not a target signal is present within a cued region of the

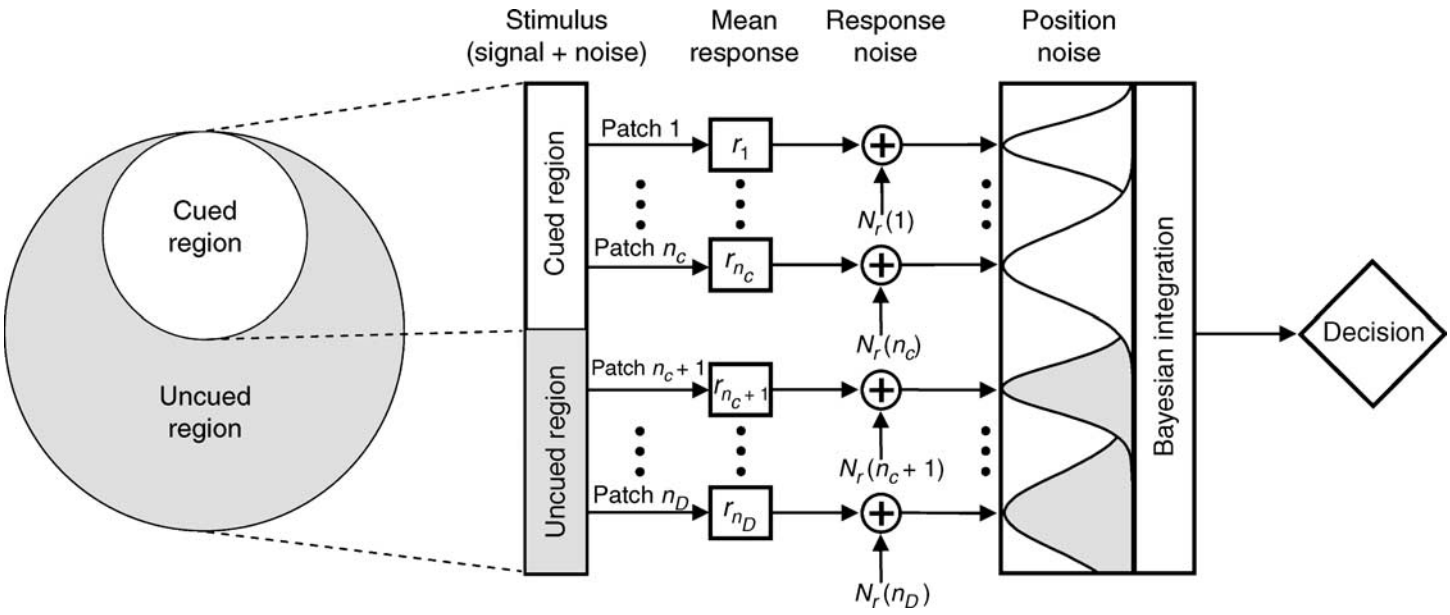

Figure 2. The intrinsic uncertainty observer. The nested circles on the left are a schematic representation of our display. The stimulus is modeled as a set of n_D discrete image patches. All n_D patches contain external noise and one of the n_C patches in the cued region may also contain a signal. The observer receives a feature response from each patch then adds intrinsic response noise to the response and intrinsic position noise to the patch location. To decide whether the target signal is present within the display, the observer computes a likelihood ratio for the responses, integrating across all n_D image patches, and compares the ratio to a criterion.

display and where the target signal, if present, is located. We assume that the observer receives independent feature responses from each of n_D discrete nonoverlapping spatial locations within the display. A subset comprising n_C of the n_D locations falls within the cue circle representing the possible target locations. Each of the feature responses is corrupted with intrinsic response noise and their perceived locations are perturbed with intrinsic position noise. The addition of intrinsic position noise implies that responses originating within the cue region may be perceptually displaced. Therefore, in deciding whether the target is present in the display, the observer must integrate across the entire display (rather than just the cued region), taking into account the probability that each response represents a patch from the cued region. We assume that, except for the intrinsic noise, the observer is ideal. That is, it integrates information optimally across spatial locations. The details of the intrinsic uncertainty observer are described in Appendix A. Here, we define the parameters that govern the two types of intrinsic uncertainty.

We assume that observer's intrinsic position uncertainty increases as a linear function of eccentricity:

$$\sigma_p(\varepsilon) = m_p\varepsilon. \tag{1}$$

This assumption follows from studies of spatial discrimination (Levi & Tripathy, 1996) and crowding (Pelli et al., 2004), which have repeatedly reported effects that vary approximately linearly with eccentricity.

Because the level of external noise is fixed across trials, we elide the distinction between intrinsic and extrinsic response uncertainties and describe their combined effect as a function $\sigma_r(c, \varepsilon)$ of target contrast c and eccentricity ε:

$$\sigma_r(c,\varepsilon) = \frac{1}{2\Phi^{-1}\left(1 - 0.5\exp\left[-\left(\frac{c}{c_T(\varepsilon)}\right)^s\right]\right)}, \tag{2}$$

where $\Phi^{-1}(\cdot)$ represents the standard normal integral, and c_T and s, respectively, represent the contrast threshold and steepness parameters for a hypothetical localized psychometric function corrected for the observer's response bias β and intrinsic position noise σ_p (see Appendix A for derivation). We constrained the contrast thresholds to rise as an exponential function of eccentricity:

$$c_T(\varepsilon) = c_T(0)\exp(m_T\varepsilon). \tag{3}$$

This simple two-parameter model has been shown to account for peripheral contrast detection thresholds across a wide variety of tasks and stimuli (Peli, Yang, & Goldstein, 1991). In total, these two components of the model require estimating 5 parameters $\{m_p, m_T, c_T(0), s, \beta\}$. We estimated the intrinsic uncertainty coefficient m_p directly from the observers' localization errors (see Estimating intrinsic position uncertainty section). The remaining parameters were estimated via a maximum

likelihood procedure from the psychometric functions measured in the conditions without extrinsic uncertainty (i.e., the Location-Specified conditions).

Results

Estimating intrinsic position uncertainty

We used the human observers' localization performance in the Location-Uncertain condition to estimate their intrinsic position uncertainty. The schematic in Figure 3 illustrates the idea behind our approach. The dotted line at the top of the figure represents the extrinsic position uncertainty introduced by randomizing the location at which the target will appear on a given trial. In a noisy detection task, this extrinsic position uncertainty leads to target mislocalizations because, even in the absence of any intrinsic position uncertainty, the observer will occasionally mistake one of the noise responses for the signal. The solid curve in Figure 3 illustrates how the frequency of mislocalizations, reflected in the localization error, varies with some measure of signal strength, such as target contrast. As the signal strength decreases, detections are increasingly dominated by such mislocalizations, leading to increasing localization error. Eventually, at zero contrast, the localization error is limited only by the extrinsic position uncertainty. Conversely, as the signal strength increases, the proportion of mislocalizations decreases. When the contrast is large enough that the target is almost surely detected on every signal trial, localization is limited only by intrinsic position uncertainty. For an observer without any intrinsic position noise, this localization error would asymptote to zero.

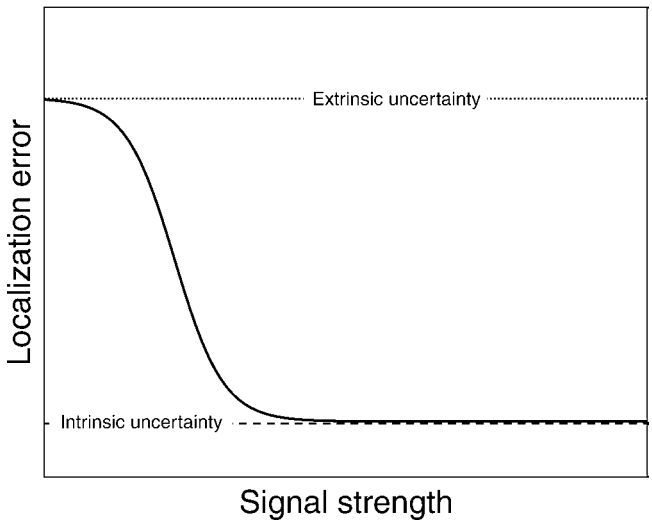

Figure 3. Expected relationship between localization error and signal strength. When the signal strength (e.g., target contrast) is low, detections are driven primarily by noise responses (i.e., "false hits") and localization performance asymptotes toward the extrinsic target Location Uncertainty (dotted line, top). As the signal strength increases, detections are increasingly dominated by signal responses (i.e., "true hits") and localization performance is asymptotically limited only by the observer's intrinsic uncertainty (dashed line, bottom).

Figure 4 shows the localization performance of the human observers for each of the individual eccentricity conditions. We used normalized target contrast (c/c_T) as the measure of signal strength. Localizations from hit trials were aggregated across subjects and binned by normalized target contrast into 20 quantiles. The dots represent the standard deviation (σ_{loc}) of the localization error in each bin, while each of the solid curves represents the least squares fit to the data for a reversed logistic function forced to pass through the standard deviation of the target location distribution (i.e., a uniform disk distribution with radius $r = \varepsilon/2$).[1] The localization errors do not go to zero but asymptote.

As indicated in Equation 1, we expected the intrinsic position uncertainty to increase linearly with eccentricity so that it could be characterized by a single parameter, the intrinsic position uncertainty coefficient $m_p = \sigma_p/\varepsilon$. To estimate this parameter across eccentricities, we normalized the localization data by calculating the *normalized localization error* (σ_{loc}/ε) from the data at each eccentricity.

Recall that the task is structured such that the cue radius defining the extrinsic uncertainty increases linearly with the eccentricity. Consequently, the standard deviation of the target location σ_{ext} across trials also increases linearly with eccentricity and we can define an extrinsic position uncertainty coefficient $m_{ext} = \sigma_{ext}/\varepsilon$ analogous to m_p that remains constant across eccentricity conditions. At low contrasts, the normalized localization error approaches m_{ext}, at high contrasts, the normalized error asymptotes at m_p. Thus, we expected that the normalized location errors for each of the eccentricities should overlap, at least at the asymptotes. Figure 5 plots these normalized localization errors across eccentricity conditions. The overlap of the data—particularly the high-contrast asymptotes—across eccentricities supports our assumption in Equation 1 that the intrinsic position uncertainty changes linearly with eccentricity (i.e., that m_p is approximately constant across eccentricity). A Chow (1960) test found no significant difference between the individual fits, $F(4, 64) = 1.67$, $p = 0.17$. On average across eccentricities, $\hat{m}_p \cong 0.09$.

So far, we have described intrinsic position noise using a single parameter σ_p, which represents the geometric mean of the standard deviations along the radial (fixation-to-target) and tangential axes. In fact, as shown in Figure 6, we found that human localization errors were anisotropic, showing greater variance along the radial axis ρ than along the tangential axis τ, with $\sigma_\rho:\sigma_\tau \approx 4:3$ across all eccentricities. Preliminary data gathered along the horizontal meridian show a nearly identical relationship,

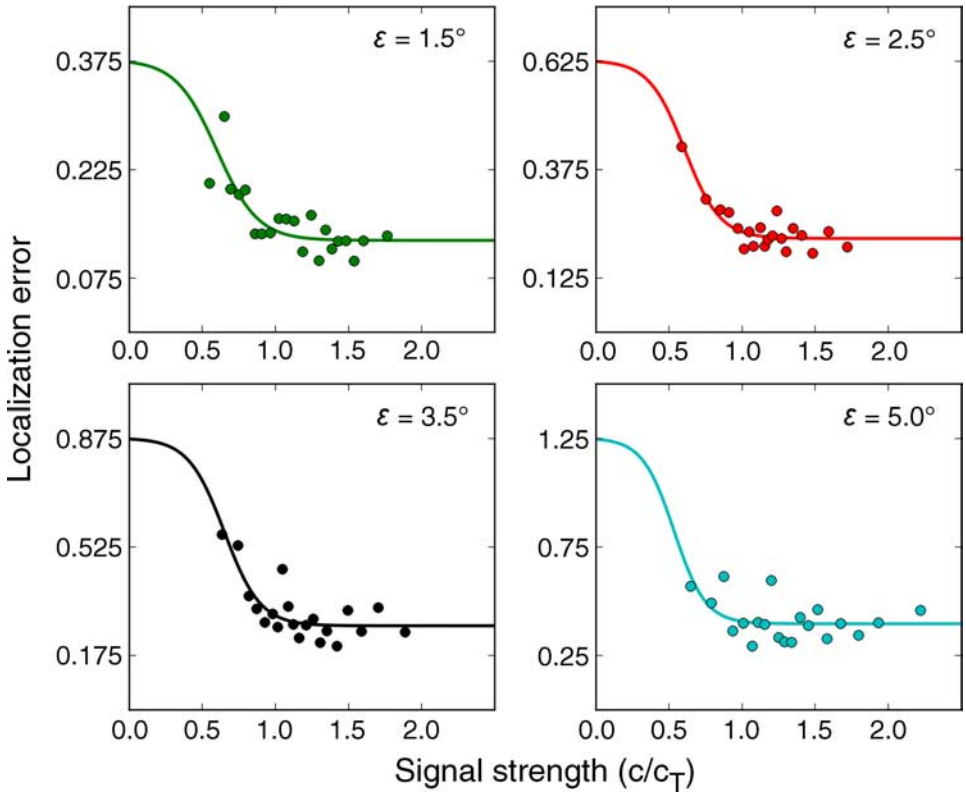

Figure 4. Observed relationship between signal strength (c/c_T) and localization error (in degrees) at each of the four eccentricities tested in the Location-Uncertain condition. Note the differences in vertical scales.

confirming that these data indeed reflect the result of a radial/tangential anisotropy (i.e., rather than that of a vertical/horizontal anisotropy). Moreover, this radial/tangential anisotropy is consistent with results from position discrimination (Klein & Levi, 1987; White, Levi, & Aitsebaomo, 1992; Yap, Levi, & Klein, 1987) and crowding (Pelli et al., 2007; Petrov & Popple, 2007; Toet & Levi, 1992) studies, though somewhat less pronounced.

Detection performance

We found that performance was similar across our three observers and combined their data to estimate parameters for the intrinsic uncertainty observer (the leftmost plot in Figure 9, along with Table 1, shows how the quality of the fit varies across individual observers). Figure 7A shows detection performance in the Location-Specified condition. The upper panel plots hits and the lower panel plots false alarms. In each panel, the dots represent the aggregate performance of the human observers and the solid curves represent the performance of the intrinsic uncertainty observer with maximum likelihood intrinsic uncertainty parameter estimates $\{\hat{m}_p = 0.09, \hat{m}_T = 0.022, \hat{c}_T(0) = 0.046, \hat{s} = 2.23, \hat{\beta} = 0.23\}$. The sizes of the dots indicate the number of (target or noise) trials they represent, and the different eccentricity conditions are coded by color. The shaded regions represent 95% binomial confidence intervals. The steepness of the observers' psychometric functions seems to increase with eccentricity. Previous work (Najemnik & Geisler, 2005) modeled this increase by allowing the steepness parameter

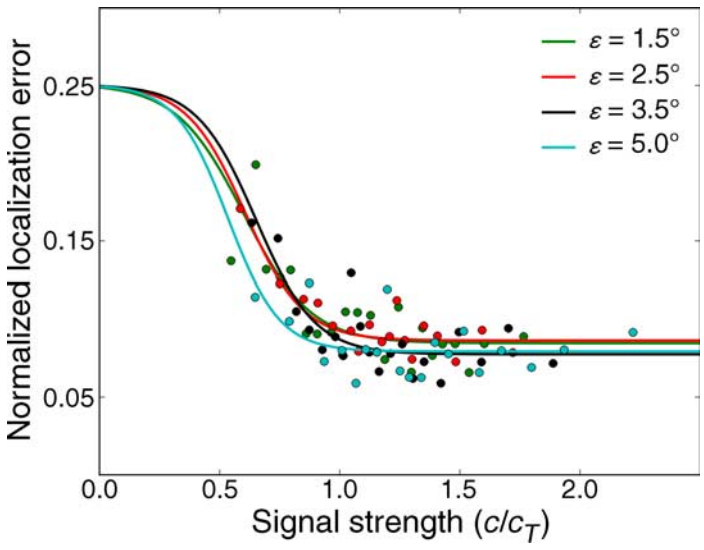

Figure 5. The observed relationship between signal strength and normalized localization error compared across eccentricities. The dot symbols each represent the normalized localization error (σ_{loc}/ε) for the indicated signal strength (c/c_T).

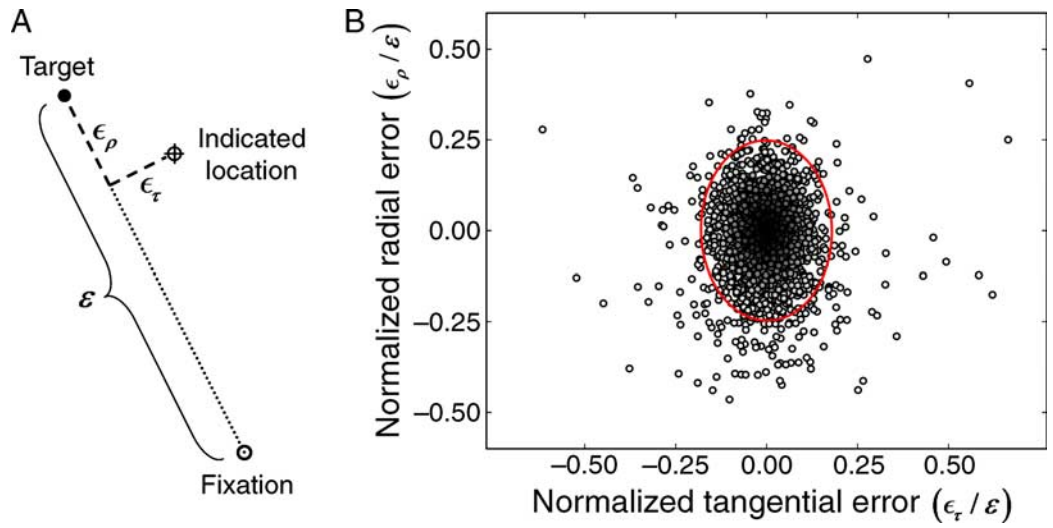

Figure 6. Anisotropy of human localization errors. (A) Schematic demonstrating tangential (ϵ_τ) and radial (ϵ_ρ) components of localization error. (B) Distribution of normalized localization errors. Each data point represents a localization error on a single hit trial. The red ellipse, representing points at a Mahalanobis distance of 2.0, illustrates the covariance of the maximum likelihood Gaussian distribution.

s to vary as a function of eccentricity. However, in the intrinsic uncertainty observer we fit only a single steepness parameter across all eccentricities. The increase in steepness for the intrinsic uncertainty observer (solid curves) reflects solely the effect of the increasing intrinsic position uncertainty estimated from human localization performance (Figure 5). To illustrate the effect of the intrinsic position uncertainty, the dashed curves in Figure 7B show the performance of a simulated observer with the same intrinsic response noise as the intrinsic uncertainty observer, but with no intrinsic position noise. As the eccentricity increases, the model without intrinsic position uncertainty does an increasingly poorer job of accounting for the human data.[2] The important result shown here is that the effect of the intrinsic position uncertainty coefficient m_p, estimated independently using localization data from the Location-Uncertain condition, is sufficient to account for the increase in the steepness of the psychometric functions with eccentricity.

Figure 8A shows the detection performance for the Location-Uncertain condition. Again, the dots represent the performance of human observers and the solid curves represent the performance of the intrinsic uncertainty observer. The parameters used for the ideal observer are the same as those used for the Location-Specified condition. Again, the intrinsic position uncertainty observer (IPU) provides a reasonably good account of the psychometric data. For comparison, the dashed curves in Figure 8B show performance of an ideal observer with no intrinsic position uncertainty (NPU) whose detection performance in the Location-Specified condition is matched to that of the human observers by allowing the steepness parameter to vary as a function of eccentricity. Here, the alternative model, lacking intrinsic position uncertainty, exaggerates the effect of extrinsic position uncertainty.

Figure 9 (center and right panels) illustrates the difference in the fidelity of the predictions of the IPU and NPU models across individual observers by plotting the predicted detection probabilities against the observed detection probabilities for each model, aggregated over cue eccentricities. Each dot represents a fifty-trial block and each color represents a different human observer. Table 1 reports the r^2 (i.e., proportion of variance explained) values for each observer and condition. A nonparametric bootstrap test[3] for equivalence of these r^2 values across the IPU and NPU models found that the differences were significant both for the combined subject data ($p < 0.001$) and for the individual observers (MMM: $p < 0.001$, TUB: $p = 0.03$; XNN: $p = 0.044$).

	Observer			
Condition (model)	MMM	TUB	XNN	Combined
Location-Specified (IPU)	0.9613	0.9542	0.8801	0.9323
Location-Uncertain (IPU)	0.9040	0.8321	0.9081	0.8826
Location-Uncertain (NPU)	0.6065	0.6883	0.7980	0.7071

Table 1. R^2 values for Figure 9.

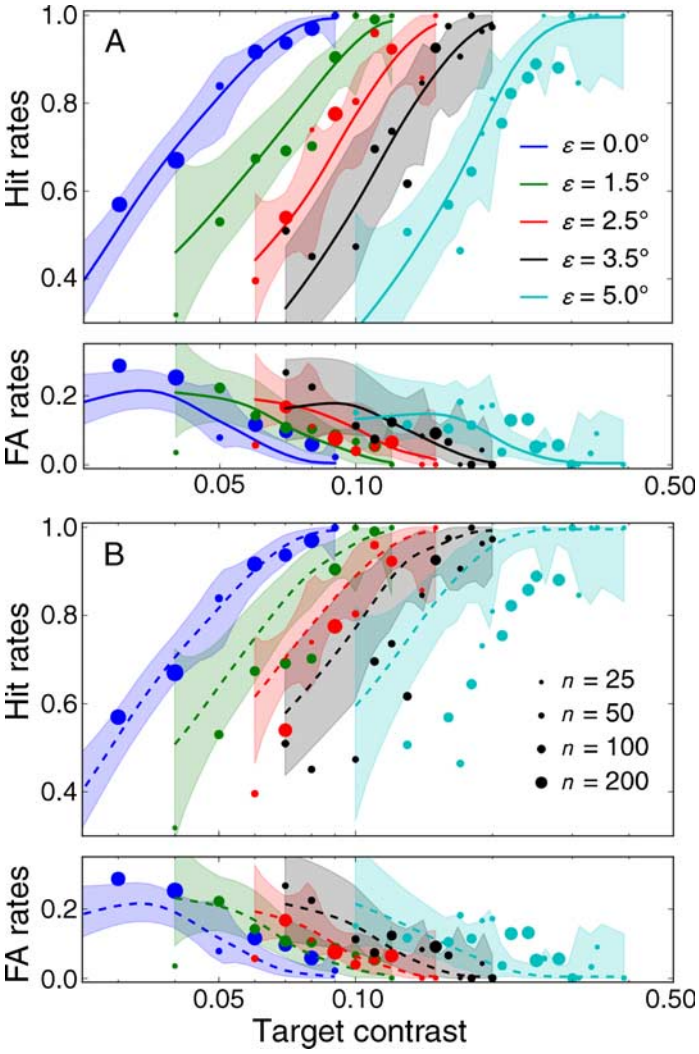

Figure 7. Comparison of human and simulated detection performances in the Location-Specified condition. Dots, aggregated human performance; curves, intrinsic uncertainty observer performance; shaded regions, 95% confidence intervals. The upper panels plot hit rates and the lower panels plot false alarm rates. (A) Detection performance for the intrinsic uncertainty observer (solid curves). (B) Detection performance for an otherwise identical observer when intrinsic position uncertainty is removed (dashed curves).

Localization performance

In addition to simulating detection performance for the intrinsic uncertainty observer, we also simulated localization performance, where the intrinsic uncertainty observer's goal is to minimize the mean squared error of the estimated location of the target (on trials where the target is detected). In this case, the estimated location is the expected value of the posterior probability distribution of target location over the cued region (see Appendix A). The dots in Figure 10 show the localization performance of the intrinsic uncertainty observer. As with the human data presented in Figure 5, the dots represent the standard deviation of the normalized localization errors (σ_{loc}/ε) as a function of normalized contrast (c/c_T), and the data are collapsed across eccentricities. The solid curve represents the best fit of a reversed logistic function to the combined human data in Figure 5. Two features of these results are worth highlighting. The first is that the asymptotic localization performance of the intrinsic uncertainty observer closely matches that of the human observers. The second is that, as with the human observers, localization errors increase with decreasing signal strength. Both of these results are anticipated in the Estimating intrinsic position uncertainty section (see Figure 3). Nonetheless, these

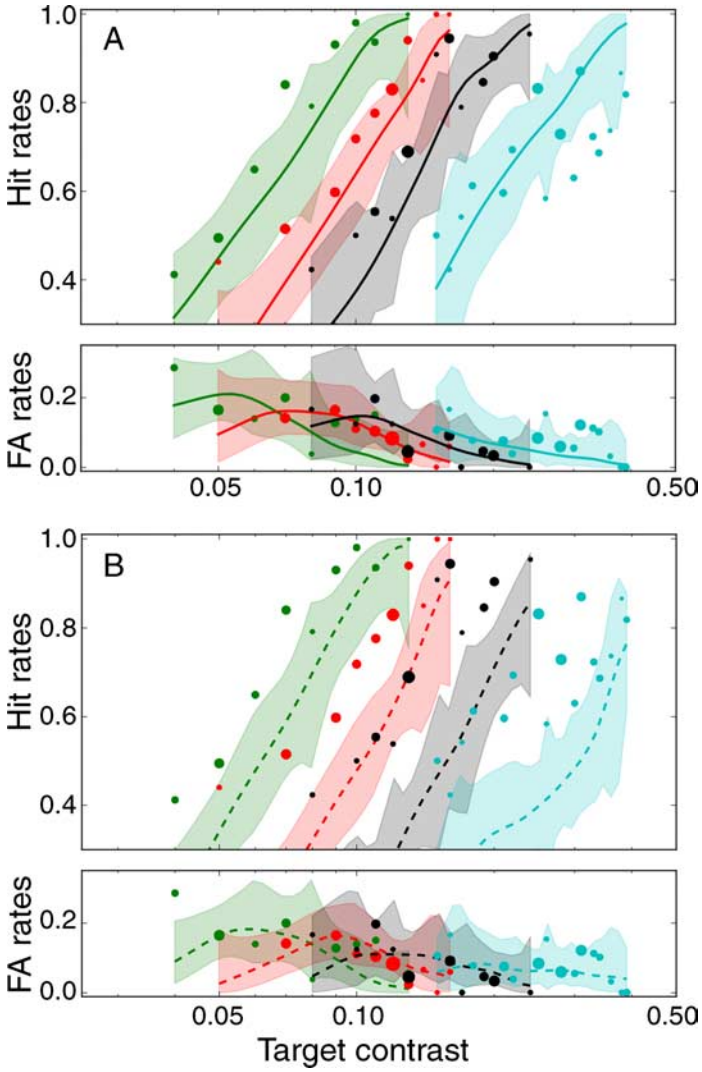

Figure 8. Comparison of human and simulated detection performances in the Location-Uncertain condition. (A) Detection performance for the intrinsic uncertainty observer (solid curves). (B) Detection performance for a simulated observer without intrinsic position uncertainty forced to match human performance in the Location-Specified condition (dashed curves).

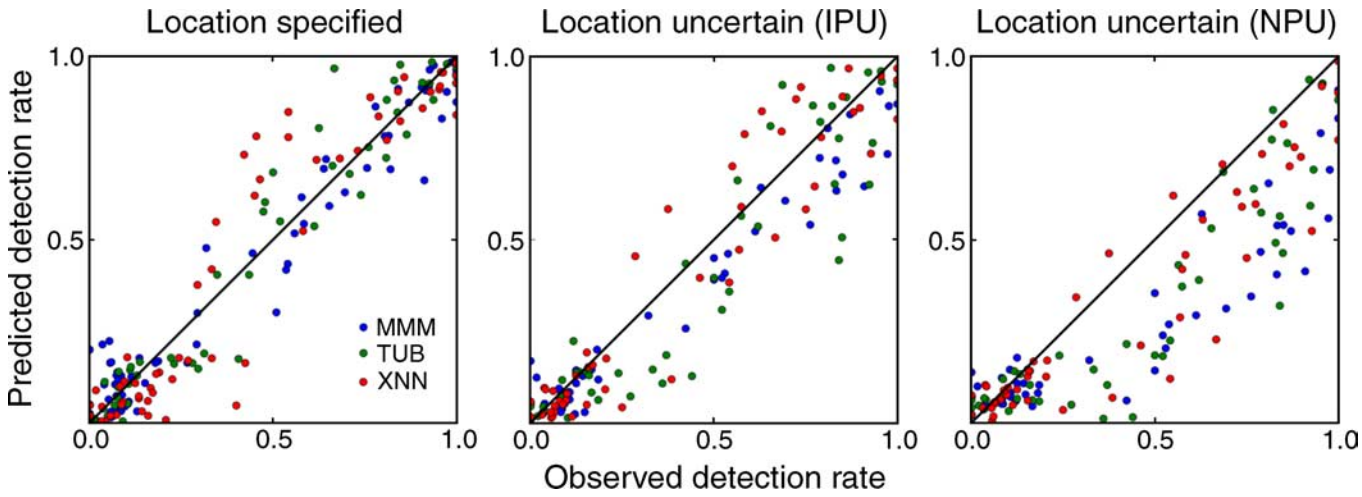

Figure 9. Comparison of individual human and simulated detection rates. Each dot marker represents the result of a 50-trial block and each color represents a different human observer. The leftmost plot represents the predicted detection rate of the intrinsic uncertainty observer as a function of the observed detection rate for each block. The central plot represents the predicted detection rate of the intrinsic uncertainty observer plotted as a function of the observed detection rate for each block. The rightmost plot represents the predicted detection rate of an alternative simulated observer with no intrinsic uncertainty whose performance in the Location-Specified condition is matched to that of the human observers.

results are important because they show that an ideal observer model in which intrinsic position uncertainty is independent of target contrast can account for the observed increase in localization error with decreasing contrast.

The plots in Figures 11 and 12 provide an alternative characterization of the detection and localization performance of human and simulated observers. In Figure 11, the data have been collapsed across the different eccentricity conditions, but the center of mass for each of the individual conditions is indicated by the corresponding number (e.g., 1.5 for 1.5-degree condition). Figure 12 shows the data of Figure 11 collapsed across different directions to show the relative density of locations as a function of distance from the center of the cued region. The top two panels of Figure 11 compare the distribution of actual target locations within the cued region on trials where the target was detected (hits) for the human and simulated observers. These two distributions appear nearly identical and show no evidence of systematic differences between the relative positions of the targets detected by the human observer and those detected by the intrinsic uncertainty observer. To quantify this result, we performed a two-dimensional version of the Kolmogorov–Smirnov test for the equality of two samples (Fasano & Franceschini, 1987) comparing the empirical distribution for the human observer with the distribution resulting from twenty runs of the simulated observer. The test showed no significant difference between the distributions, $D(1880, 34859) = 0.023$, $p = 0.57$. The left-hand plot in Figure 12 provides an additional view of the similarity of these distributions. However, the lower two panels in Figure 11 reveal differences in localization between the human and simulated observers, $D(1880, 34859) = 0.122$, $p < 0.001$. In particular, the human observers show systematically biased pointing behaviors. At small eccentricities, human observers tend to bias their pointing toward the fovea. This bias tapers off at about 3.0 degrees, after which subjects tend to bias their pointing behaviors away from the fovea. This modest bias may have been induced by the landmark cues provided by the fixation

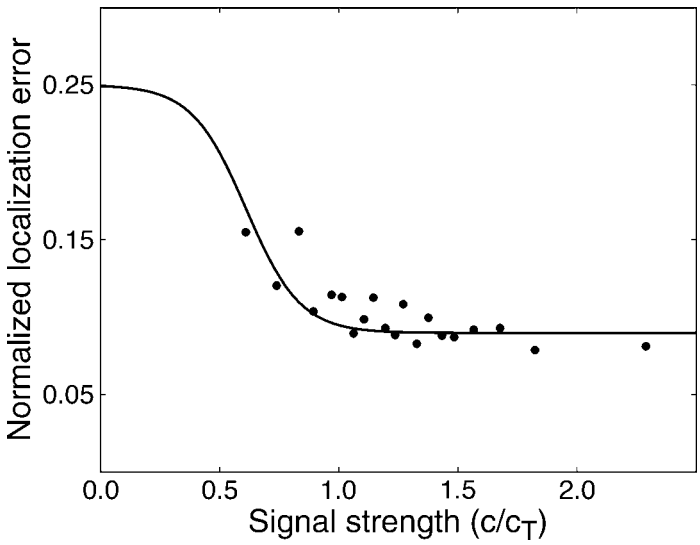

Figure 10. The observed relationship between signal strength (c/c_T) and normalized localization error (σ_{loc}/ε) for the intrinsic uncertainty observer. Dots, localization errors for the intrinsic uncertainty observer; solid curve, fit to human localization errors in Figure 5.

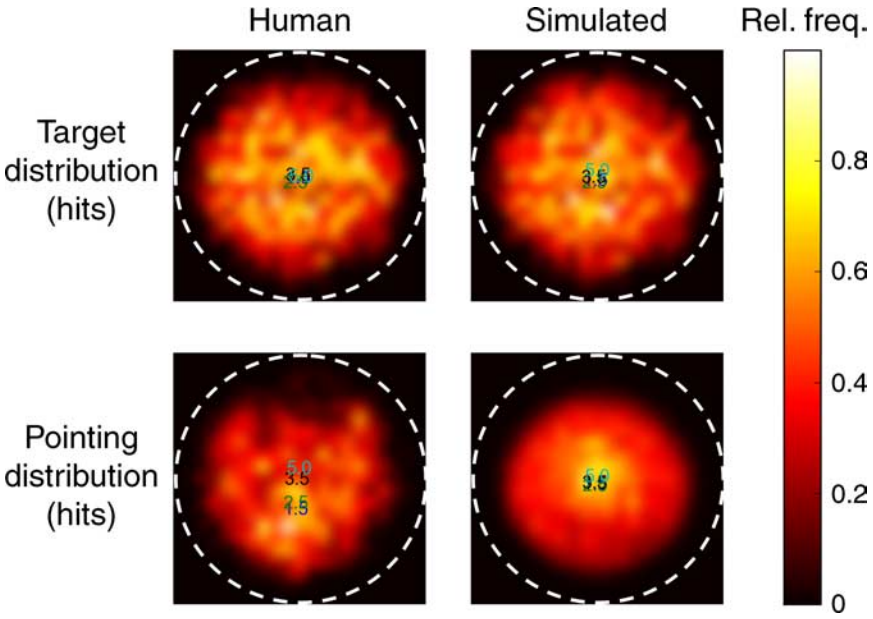

Figure 11. Comparison of detected target location and pointing distributions within the cued region for human and intrinsic uncertainty observers. The plots represent the distribution of locations relative to the cued region, whose boundary is indicated by the dashed white circle. The data are collapsed across eccentricity conditions, but the center of mass for the individual conditions is indicated by the placement of the corresponding numbers.

marker and the frame of the monitor (Diedrichsen, Werner, Schmidt, & Trommershauser, 2004; Werner & Diedrichsen, 2002), both of which were visible throughout each trial. Nonetheless, despite this bias, the asymptotic localization errors remain approximately equal between the human and simulated observers.

Discussion

The primary aim of the current study was to determine how the effective intrinsic position uncertainty of human observers performing a detection task changes as a function of retinal eccentricity. We estimated intrinsic position uncertainty from the asymptotic localization performance of our human observers and estimated intrinsic response uncertainty from their detection performance in a task without any extrinsic position uncertainty. We found that the estimated intrinsic position uncertainty, when incorporated into a constrained ideal observer, predicts performance in a task with extrinsic position uncertainty, accounting for the reduced impact of external position uncertainty with eccentricity that a model without intrinsic position uncertainty does not predict. In addition, we found that the intrinsic observer accounts for several additional features of human performance including the increase in steepness of the psychometric function with eccentricity and the spatial distribution of detected targets.

Consequences of intrinsic position uncertainty

The intrinsic position uncertainty model resembles and draws upon elements of previous models of inefficiencies in the human visual system, such as equivalent-noise models (e.g., Ahumada & Watson, 1985; Lu & Dosher, 1999) and maximum-of-outputs uncertainty models (e.g., Green & Swets, 1966; Pelli, 1985; Swensson & Judy, 1981) of contrast detection and discrimination. Indeed, a

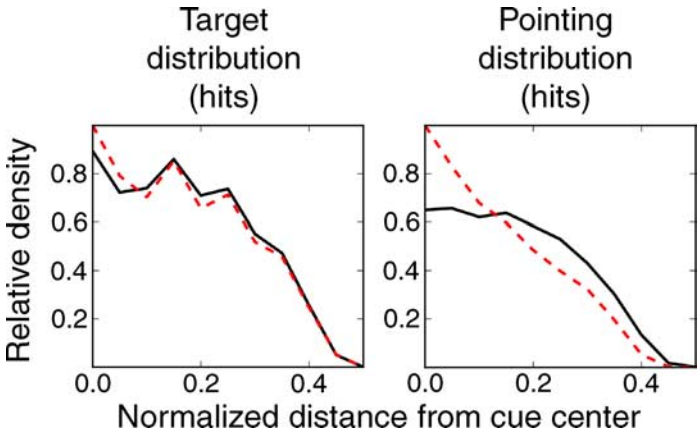

Figure 12. Relative density of detected target and pointing locations. Solid black curves, human observers; dashed red curves, intrinsic uncertainty observer. These are the data from Figure 11 replotted in terms of relative density as a function of normalized distance from the cue center.

straightforward equivalent-noise model could account for the detection performance in the Location-Specified condition of our task by allowing the steepness parameter of the psychometric functions to vary as a function of eccentricity (e.g., as in Najemnik & Geisler, 2005), and a maximum-of-outputs model could account for the same results by allowing M, the number of possible signals, to vary as a function of eccentricity. The intrinsic position uncertainty model differs from these models in that it distinguishes the uncertainty due to intrinsic position uncertainty from that due to other forms of uncertainty. To be sure, other authors have suggested models of intrinsic inefficiency that use equivalent noise combined with intrinsic signal uncertainty (including position uncertainty) to account for nonlinearities in the psychometric function (e.g., Beutter, Eckstein, & Stone, 2003; Eckstein, Ahumada, & Watson, 1997; Zhang, Pham, & Eckstein, 2006) or to quantify the efficacy of various target location cues (Manjeshwar & Wilson, 2001). However, the intrinsic position uncertainty model is unique in that it represents the interaction between intrinsic and extrinsic position uncertainties as a function of peripheral eccentricity, anticipating the reduced impact of extrinsic position uncertainty on detection performance that results from increasing intrinsic position uncertainty. Figure 8B shows how an equivalent-noise model with steepness and threshold parameters fit to match detection performance in the Location-Specified condition fails to account for performance in the Location-Uncertain condition.

More generally, the failure of the equivalent-noise model in Figure 8B illustrates the importance of intrinsic position uncertainty in determining detection performance. In visual search and uncertainty experiments, researchers often estimate equivalent noise (or a proxy) by measuring detection performance in a display containing one—two in the case of forced choice tasks—specified target location (e.g., Burgess & Ghandeharian, 1984; Cameron et al., 2004; Cohn & Wardlaw, 1985; Eckstein & Whiting, 1996; Michel & Geisler, 2009; Najemnik & Geisler, 2005; Palmer et al., 2000; Swensson & Judy, 1981). They then use these estimates to determine the relative efficiency of human observers or to otherwise compare human performance to that of an optimal searcher or detector limited by the equivalent noise in the search or uncertainty task. When intrinsic position noise is ignored, this technique can potentially lead to erroneous conclusions. For example, detection performance matching the dashed curves in Figure 8B would be interpreted as optimal under such a framework.

Comparison with results from position discrimination and crowding studies

Certain patterns in the measured human localization errors and in our estimates of intrinsic position noise share qualitative similarities with patterns observed for discrimination thresholds in position discrimination studies and for "critical spacing" regions in crowding studies. In particular, we found that the standard deviation of the intrinsic position noise, like position discrimination thresholds (e.g., Klein & Levi, 1987; Levi & Tripathy, 1996; White et al., 1992) and crowding regions (e.g., Bouma, 1970; Levi, 2008; Levi, Hariharan, & Klein, 2002; Pelli, 2008), increases approximately linearly with eccentricity. We also found that the intrinsic position uncertainty is greater in the radial direction than in the tangential direction (for position discrimination: Klein & Levi, 1987; White et al., 1992; Yap et al., 1987; for crowding: Pelli et al., 2007; Petrov & Popple, 2007; Toet & Levi, 1992).

These similarities make it tempting to suggest a common mechanism underlying these phenomena. Unfortunately, the similarities may be only superficial. The linear constant, for example, can vary by as much as two orders of magnitude between critical crowding regions and position discrimination thresholds, depending on how these are measured (see White et al., 1992, Table 2 for various estimates of this constant in position discrimination tasks, and Pelli et al., 2004, for estimates of this constant across various crowding tasks). One might be especially tempted to draw a comparison between the measurements reported in this paper and those reported in position discrimination experiments, since both of these ostensibly study intrinsic position uncertainty (Hess & Hayes, 1994; Klein & Levi, 1987). However, important differences between our experimental framework and those used in position discrimination experiments make it difficult to compare results or even to determine whether both are measuring related phenomena. First, studies of position discrimination typically involve fine one-dimensional judgments of the relative alignment of two or three elements (e.g., Hess & Field, 1993; Hess & Hayes, 1994; Klein & Levi, 1987; Levi, Klein, & Yap, 1987; Levi & Klein, 1990; Westheimer, 1982), tasks that may involve secondary cues to position such as local contrast, phase, orientation, or curvature, rather than the spatial localization of feature elements *per se* (Sullivan, Oatley, & Sutherland, 1972; Watt, 1984; Watt & Morgan, 1984; Wilson, 1986). Second, while the current study measures feature localization near threshold contrasts in spatial noise, position discrimination tasks use effectively zero-contrast backgrounds with elements whose contrasts can range from about 2 (Hess & Hayes, 1994; Levi & Tripathy, 1996) to as much as 50 (White et al., 1992) times the detection threshold. The exclusion of any sort of textured background in these studies is especially important considering that the introduction of just a single distracter element can substantially influence localization judgments in position discrimination tasks (Burbeck & Hadden, 1993; Hess & Badcock, 1995). Our goal in the current study was not, as in position discrimination experiments, to determine the minimum spatial offset that

human observers can detect between elements under ideal conditions but rather their effective uncertainty with respect to the locations of features in a detection task.

Conclusion

This study introduced a *dual-response* detection task where subjects report not only when a target is detected but its apparent location. The large amount of additional information provided by this task strongly constrains models of detection performance, and it revealed clear evidence that position uncertainty is an important factor limiting detection performance in the periphery. This study also introduced a new ideal observer model for detection, the *intrinsic uncertainty observer*, which may serve as the foundation for improved models of peripheral vision. This is potentially important because accurate models of peripheral vision are critical for understanding and predicting performance in natural visual tasks, which typically involve controlling the direction of gaze based on information detected in the periphery.

Appendix A

Derivation of intrinsic uncertainty observer

Characterizing the visual system

Consider the ideal detector for a signal-known-exactly in a simple detection task. Each stimulus presentation consists either of noise alone or of noise plus a signal. The ideal detector computes the cross-correlation of the display with a prewhitened matched template of the target to obtain a scalar-valued template response R, which is then compared to a criterion. If R exceeds the criterion, the detector responds "target present"; otherwise, it responds "target absent." Ideal performance in this task varies monotonically with the signal-to-noise ratio d', which, in the current task, is manipulated by varying the contrast c of the target signal:

$$d'(c) = 2\Phi^{-1}[\mathrm{PC}_{\max}(c)], \tag{A1}$$

where $\Phi^{-1}[\cdot]$ represents the inverse of the standard normal integral and $\mathrm{PC}_{\max}(c)$ is a psychometric function representing the proportion-correct detection performance for an observer whose goal is to minimize detection errors (i.e., false alarms + misses). The psychometric function is modeled as a cumulative Weibull function with two parameters: a contrast threshold parameter c_T and a steepness parameter s:

$$\mathrm{PC}_{\max}(c) = 1 - 0.5\exp\left[-\left(\frac{c}{c_T}\right)^s\right]. \tag{A2}$$

In human observers, due largely to inhomogeneities in retinal sampling and cortical representation, the contrast threshold varies as a function of the target's position in the retinal image. We assume that the threshold changes as an exponential function of retinal eccentricity (Peli et al., 1991):

$$c_T(\varepsilon) = c_T(0)\exp(m_T\varepsilon). \tag{A3}$$

Combining Equations A1 and A2, we describe the effective signal-to-noise ratio for a human observer detecting a signal-known-exactly:

$$d'(c,\varepsilon) = 2\Phi^{-1}\left(1 - 0.5\exp\left[-\left(\frac{c}{c_T(\varepsilon)}\right)^s\right]\right). \tag{A4}$$

We compute the effective response noise $\sigma_r(c, \varepsilon)$ by assuming that the difference between the signal and noise response means is fixed to 1. In this case, $\sigma_r(c, \varepsilon) = 1/d'(c, \varepsilon)$, which leads to the result in Equation 2 of the main text:

$$\sigma_r(c,\varepsilon) = \frac{1}{2\Phi^{-1}\left(1 - 0.5\exp\left[-\left(\frac{c}{c_T(\varepsilon)}\right)^s\right]\right)}. \tag{A5}$$

However, even when the signal is specified exactly, human observers behave as though some of the stimulus parameters are uncertain (Tanner, 1961). One of the parameters for which humans demonstrate intrinsic uncertainty is stimulus position. We represent this uncertainty by modeling an intrinsic position noise whose standard deviation σ_p varies as a linear function of eccentricity:

$$\sigma_p(\varepsilon) = m_p\varepsilon. \tag{A6}$$

We estimated the linear coefficient $\hat{m}_p = 0.09$ from the asymptotic localization performance of the human observers. Moreover, we found that this intrinsic noise is anisotropic, with greater variance along the radial axis ρ (i.e., the direction of increasing retinal eccentricity) than along the tangential axis τ (perpendicular to the radial axis). The ratio of noise along each axis appears constant across eccentricities with

$$\sigma_\tau(\varepsilon) = 0.87\sigma_p(\varepsilon), \tag{A7}$$

and

$$\sigma_p(\varepsilon) = 1.15\sigma_p(\varepsilon). \quad \text{(A8)}$$

Note that the resulting covariance matrix $\Sigma_p(\varepsilon, \theta)$ now varies as a function of direction. After estimating the intrinsic uncertainty parameter, we estimated the parameters describing the effective response noise (i.e., $c_T(0)$, m_T, s) from the detection performance in the Location-Specified condition using a maximum likelihood procedure described in the Simulation of the intrinsic uncertainty observer section. Note that our procedure for estimating the response noise parameters took into account the effect of the intrinsic position uncertainty on detection performance.

Representing the display

During the stimulus interval, the observer receives responses from each of the n_D discrete spatial locations within the display. A subset of these, comprising n_C locations, falls within the cue circle representing possible target locations. Let R_i be the response obtained from display location (x_i, y_i), where i indexes the display locations and $R_i = r_i + N_r(i)$ and $N_r(i)$ is Gaussian noise with mean 0 and standard deviation $\sigma_r(i)$. In addition, let J be the target location chosen randomly from among the n_C possible target locations. For mathematical convenience and without loss of generality, we assume that $r_i = 0.5$ if $i = J$ and $r_i = -0.5$ otherwise.

Let $(X_i, Y_i) = (x_i, y_i) + (N_x(i), N_y(i))$ be the encoded location of the response R_i, where $(N_x(i), N_y(i))$ is Gaussian noise with mean 0 and covariance matrix $\Sigma_p(i)$. Finally, to simplify notation, let $\mathbf{W}_i = [R_i, X_i, Y_i]$. Because randomly changing the position of a noise patch has no effect on the decision or performance, we can assume that $\mathbf{W}_i = [R_i, x_i, y_i]$ for all $i \neq J$ and $\mathbf{W}_J = [R_J, X_J, Y_J]$. In simulations, we represented the display as a triangular array of nonoverlapping patches whose centers were spaced 0.6° apart (the diameter of the target signal).

Optimal detection

The intrinsic uncertainty observer integrates optimally across spatial locations to decide whether the target signal is present within the display.

The optimal decision rule is to compute the likelihood ratio:

$$l(\mathbf{W}_1, \ldots, \mathbf{W}_{n_D}) = \frac{p(\mathbf{W}_1, \ldots, \mathbf{W}_{n_D}|\text{signal})}{p(\mathbf{W}_1, \ldots, \mathbf{W}_{n_D}|\text{noise})}, \quad \text{(A9)}$$

and compare it to a criterion β (Green & Swets, 1966).

The likelihood that the target is present is

$$p(\mathbf{W}_1, \ldots, \mathbf{W}_{n_D}|\text{signal}) = \sum_{k=1}^{n_D}\sum_{j=1}^{n_C} p(\mathbf{W}_1, \ldots, \mathbf{W}_{n_D}|\text{signal}, j, k) \cdot p(k|j)p(j), \quad \text{(A10)}$$

$$p(\mathbf{W}_1, \ldots, \mathbf{W}_{n_D}|\text{signal}) = \sum_{k=1}^{n_D}\sum_{j=1}^{n_C} p(k|j)p(j) \cdot \prod_{i=1}^{n_D} p(\mathbf{W}_i|\text{signal}, j, k), \quad \text{(A11)}$$

where

$$p(\mathbf{W}_i|\text{signal}, j, k) = \begin{cases} \frac{1}{\sqrt{2\pi}\sigma_r(i)}\exp\left[-\frac{(R_i+0.5)^2}{2\sigma_r^2(i)}\right] & i \neq k \\ \frac{1}{\sqrt{2\pi}\sigma_r(j)}\exp\left[-\frac{(R_i-0.5)^2}{2\sigma_r^2(j)}\right] & i = k \end{cases}. \quad \text{(A12)}$$

Here, j indexes over possible target patches, k indexes over encoded responses, $p(j) = 1/n_C$ represents the prior probability that the target was located in patch j, and $p(k|j)$ represents the probability that the encoded location (X_k, Y_k) of R_k was actually generated by patch j in the display. Note that because the encoded locations in the image are binned into discrete spatial regions, this probability is computed as the integral over the region centered on (X_k, Y_k) for a Gaussian centered on the true location (x_j, y_j) with covariance $\Sigma_p(j)$.

The likelihood that the target is absent is

$$p(\mathbf{W}_1, \ldots, \mathbf{W}_{n_D}|\text{noise}) = \prod_{i=1}^{n_D} p(\mathbf{W}_i|\text{noise}), \quad \text{(A13)}$$

where

$$p(\mathbf{W}_i|\text{noise}) = \frac{1}{\sqrt{2\pi}\sigma_r(i)}\exp\left[-\frac{(R_i+0.5)^2}{2\sigma_r^2(i)}\right]. \quad \text{(A14)}$$

Substituting Equations A11 and A13 into Equation A9 yields

$$l(\mathbf{W}_1, \ldots, \mathbf{W}_{n_D}) = \sum_{k=1}^{n_D}\sum_{j=1}^{n_C} p(k|j)p(j)\prod_{i=1}^{n_D}\frac{p(\mathbf{W}_i|\text{signal}, j, k)}{p(\mathbf{W}_i|\text{noise})}. \quad \text{(A15)}$$

Furthermore, since $p(\mathbf{W}_i \mid \text{signal}, j, k) = p(\mathbf{W}_i \mid \text{noise})$ for $i \neq k$,

$$l(\mathbf{W}_1, \ldots, \mathbf{W}_{n_D}) = \sum_{k=1}^{n_D} \sum_{j=1}^{n_C} p(k|j)p(j) \frac{p(\mathbf{W}_k|\text{signal}, j, k)}{p(\mathbf{W}_k|\text{noise})}, \tag{A16}$$

$$l(\mathbf{W}_1, \ldots, \mathbf{W}_{n_D}) = \sum_{k=1}^{n_D} \sum_{j=1}^{n_C} p(k|j)p(j) \frac{\sigma_r(k)\exp\left[-\frac{(R_k-0.5)^2}{2\sigma_r^2(j)}\right]}{\sigma_r(j)\exp\left[-\frac{(R_k+0.5)^2}{2\sigma_r^2(k)}\right]}, \tag{A17}$$

$$l(\mathbf{W}_1, \ldots, \mathbf{W}_{n_D}) = \sum_{j=1}^{n_C} p(j) \sum_{k=1}^{n_D} p(k|j) \frac{\sigma_r(k)}{\sigma_r(j)} \cdot \exp\left[\frac{(R_k+0.5)^2}{2\sigma_r^2(k)} - \frac{(R_k-0.5)^2}{2\sigma_r^2(j)}\right]. \tag{A18}$$

Optimal computation of signal location

On trials where $l(\mathbf{W}_1, \ldots, \mathbf{W}_{n_D}) > \beta$, the observer detects a target and must estimate its location. We assume that the observer's goal in the localization task is to minimize the average squared error between the true and estimated target locations. Therefore, the estimated target location $(\hat{x}, \hat{y})$ is its expected location given the observed responses $(\mathbf{W}_1, \ldots, \mathbf{W}_{n_D})$:

$$\begin{aligned}(\hat{x}, \hat{y}) &= E\left[(X_J, Y_J)|\mathbf{W}_1, \ldots, \mathbf{W}_n\right] \\ &= \sum_{j=1}^{n_C} p(j|\mathbf{W}_1, \ldots, \mathbf{W}_{n_D})(x_j, y_j),\end{aligned} \tag{A19}$$

where $E[\cdot]$ represents the expectation operator.

Using Bayes' rule,

$$(\hat{x}, \hat{y}) = \frac{\sum_{j=1}^{n_C} p(j)p(\mathbf{W}_1, \ldots, \mathbf{W}_{n_D}|j)(x_j, y_j)}{\sum_{i=1}^{n_C} p(i)p(\mathbf{W}_1, \ldots, \mathbf{W}_{n_D}|i)}. \tag{A20}$$

Now,

$$p(\mathbf{W}_1, \ldots, \mathbf{W}_{n_D}|j) = \sum_{k=1}^{n_D} p(\mathbf{W}_1, \ldots, \mathbf{W}_{n_D}|j, k)p(k|j), \tag{A21}$$

$$p(\mathbf{W}_1, \ldots, \mathbf{W}_{n_D}|j) = \sum_{k=1}^{n_D} p(k|\,j)p(\mathbf{W}_k|\text{signal}, j, k) \cdot \prod_{l\neq k} p(\mathbf{W}_l|\text{signal}, j, k), \tag{A22}$$

$$p(\mathbf{W}_1, \ldots, \mathbf{W}_{n_D}|j) = \prod_{l=1}^{n_D} p(\mathbf{W}_l|\text{noise}) \sum_{k=1}^{n_D} p(k|j) \frac{p(\mathbf{W}_k|\text{signal}, j, k)}{p(\mathbf{W}_k|\text{noise})}. \tag{A23}$$

Substituting into Equation A20

$$(\hat{x}, \hat{y}) = \frac{\sum_{j=1}^{n_C} (x_j, y_j)p(j) \sum_{k=1}^{n_D} p(k|j) \frac{p(\mathbf{W}_k|\text{signal}, j, k)}{p(\mathbf{W}_k|\text{noise})}}{\sum_{i=1}^{n_C} p(i) \sum_{k=1}^{n_D} p(k|l) \frac{p(\mathbf{W}_k|\text{signal}, i, k)}{p(\mathbf{W}_k|\text{noise})}}. \tag{A24}$$

Note that, except for the (x_j, y_j) term in the numerator, both the numerator and denominator of Equation A24 are equivalent to the likelihood term in Equations A16–A18. Thus,

$$(\hat{x}, \hat{y}) = \frac{\sum_{j=1}^{n_C} (x_j, y_j)p(j) \sum_{k=1}^{n_D} p(k|j) \frac{\sigma_r(k)}{\sigma_r(j)} \exp\left[\frac{(R_k+0.5)^2}{2\sigma_r^2(k)} - \frac{(R_k-0.5)^2}{2\sigma_r^2(j)}\right]}{l(\mathbf{W}_1, \ldots, \mathbf{W}_{n_D})}. \tag{A25}$$

Simulation of the intrinsic uncertainty observer

We used Monte Carlo simulation to estimate the detection and localization of the intrinsic uncertainty observer. In simulating each trial, we used the target location and target contrast presented to the human observer. Each trial was simulated as follows:

1. For target present trials, we set, $r_J = 0.5$ and $r_i = -0.5$ for $i \neq J$. For target absent trials, all r_i were set to -0.5.
2. Gaussian noise samples R_i were generated for each of the n_D locations in the display as described in the Representing the display section.
3. A location in the grid (X_J, Y_J) was selected randomly as the encoded target location according to $p(X_J, Y_J \mid x_J, y_J, \Sigma_p(J))$.
4. The observer decided whether the target was present in the display using Equation A18 and comparing it to the criterion β. If $l(\mathbf{W}_1, \ldots, \mathbf{W}_{n_D}) > \beta$, the observer responded "target present"; otherwise, the observer responded "target absent."

5. Finally, if the target signal was detected, the ideal observer calculated its expected location using Equation A25.

The intrinsic response noise parameters $\{m_T, c_T(0), s\}$ along with the criterion β were estimated by repeatedly simulating the intrinsic uncertainty observer with different parameter values along a four-dimensional grid and choosing the set of parameters (i.e., the point in the grid) that maximized the likelihood. The likelihoods were calculated as the probability of observing the empirical numbers of hits and false alarms given the hit and false alarm rates predicted by the intrinsic uncertainty observer. To obtain stable estimates, the predicted hit and false alarm rates were calculated by averaging over 100 runs of each block.

Acknowledgments

This work was supported by NIH Grant EY02688.

Commercial relationships: none.
Corresponding author: Melchi Michel.
Email: melchi@mail.cps.utexas.edu.
Address: Center for Perceptual Systems, University of Texas at Austin, 1 University Station A8000, Austin, TX, USA.

Footnotes

[1]This value (the standard deviation of the target location) reflects the optimal localization performance of an ideal observer whose goal is to minimize its squared localization error when the display contains no additional information about the target's location on a given trial. Thus, the values on the left-hand sides of the plots in Figure 4 represent lower bounds on human localization errors near zero contrast.

[2]Note that a model that allows the steepness parameter to vary with eccentricity, as in Najemnik and Geisler (2005), provides as good a fit to the Location-Specified data as the intrinsic uncertainty observer model. However, such a model fails to predict performance in the Location-Uncertain condition (as illustrated in Figure 8B).

[3]We tested the null hypothesis ($r^2_{IPU} = r^2_{NPU}$) by merging the data from the IPU and NPU predictions and repeatedly resampling appropriately sized samples to compute r^{*2}_{IPU} and r^{*2}_{NPU}, the coefficients of determination for the samples. After repeating this process for 50,000 iterations, we determined the proportion of samples α for which $r^{*2}_{IPU} - r^{*2}_{NPU} \geq r^2_{IPU} - r^2_{NPU}$. Finally, we used a two-tailed test for significance by setting $p = 2\alpha$.

References

Ahumada, A. J., & Watson, A. B. (1985). Equivalent-noise model for contrast detection and discrimination. *Journal of the Optical Society of America A, Optics and Image Science, 2,* 1133–1139.

Baldassi, S., & Burr, D. C. (2000). Feature-based integration of orientation signals in visual search. *Vision Research, 40,* 1293–1300.

Beutter, B. R., Eckstein, M. P., & Stone, L. S. (2003). Saccadic and perceptual performance in visual search tasks: I. Contrast detection and discrimination. *Journal of the Optical Society of America A, 20,* 1341–1355.

Bochud, F. O., Abbey, C. K., & Eckstein, M. P. (2004). Search for lesions in mammograms: Statistical characterization of observer responses. *Medical Physics, 31,* 24.

Bouma, H. (1970). Interaction effects in parafoveal letter recognition. *Nature, 226,* 177–178.

Burbeck, C. A., & Hadden, S. (1993). Scaled position integration areas: Accounting for Weber's law for separation. *Journal of the Optical Society of America A, 10,* 5–15.

Burgess, A. E., & Ghandeharian, H. (1984). Visual signal detection: II. Signal-location identification. *Journal of the Optical Society of America A, 1,* 906–910.

Burgess, A. E., Wagner, R. F., Jennings, R. J., & Barlow, H. B. (1981). Efficiency of human visual signal discrimination. *Science, 214,* 93–94.

Cameron, E. L., Tai, J. C., Eckstein, M. P., & Carrasco, M. (2004). Signal detection theory applied to three visual search tasks—Identification, yes/no detection and localization. *Spatial Vision, 17,* 295–325.

Chow, G. (1960). Tests of equality between sets of coefficients in two linear regressions. *Econometrica, 28,* 591–605.

Cohn, T., & Wardlaw, J. (1985). Effect of large spatial uncertainty on foveal luminance increment detectability. *Journal of the Optical Society of America A, 2,* 820–825.

Cohn, T. E., & Lasley, D. J. (1974). Detectability of a luminance increment: Effect of spatial uncertainty. *Journal of the Optical Society of America, 64,* 1715–1719.

Diedrichsen, J., Werner, S., Schmidt, T., & Trommershäuser, J. (2004). Immediate spatial distortions of pointing movements induced by visual landmarks. *Perception & Psychophysics, 66,* 89–103.

Eckstein, M., & Whiting, J. (1996). Visual signal detection in structured backgrounds: I. Effect of number of possible spatial locations and signal contrast. *Journal of the Optical Society of America A, 13,* 1777–1787.

Eckstein, M. P. (1998). The lower visual search efficiency for conjunctions is due to noise and not serial attentional processing. *Psychological Science, 9,* 111–118.

Eckstein, M. P., Ahumada, A. J., & Watson, A. B. (1997). Visual signal detection in structured backgrounds: II. Effects of contrast gain control, background variations, and white noise. *Journal of the Optical Society of America A, 14,* 2406–2419.

Eckstein, M. P., Thomas, J. P., Palmer, J., & Shimozaki, S. S. (2000). A signal detection model predicts the effects of set size on visual search accuracy for feature, conjunction, triple conjunction, and disjunction displays. *Perception & Psychophysics, 62,* 425–451.

Fasano, G., & Franceschini, A. (1987). A multidimensional version of the Kolmogorov–Smirnov test. *Monthly Notices of the Royal Astronomical Society, 255,* 615–627.

Green, D. M., & Swets, J. A. (1966). *Signal detection theory and psychophysics*. New York: Wiley.

Hess, R., & Field, D. (1993). Is the increased spatial uncertainty in the normal periphery due to spatial undersampling or uncalibrated disarray? *Vision Research, 33,* 2663–2670.

Hess, R. F., & Badcock, D. R. (1995). Metric for separation discrimination by the human visual system. *Journal of the Optical Society of America A, 12,* 3–16.

Hess, R. F., & Hayes, A. (1994). The coding of spatial position by the human visual system: Effects of spatial scale and retinal eccentricity. *Vision Research, 34,* 625–643.

Klein, S. A., & Levi, D. M. (1987). Position sense of the peripheral retina. *Journal of the Optical Society of America A, 4,* 1543–1553.

Levi, D., Klein, S., & Yap, Y. L. (1987). Position uncertainty in peripheral and amblyopic vision. *Vision Research, 27,* 581–597.

Levi, D. M. (2008). Crowding—An essential bottleneck for object recognition: A mini-review. *Vision Research, 48,* 635–654.

Levi, D. M., Hariharan, S., & Klein, S. A. (2002). Suppressive and facilitatory spatial interactions in peripheral vision: Peripheral crowding is neither size invariant nor simple contrast masking. *Journal of Vision, 2*(2):3, 167–177, http://www.journalofvision.org/content/2/2/3, doi:10.1167/2.2.3. [PubMed] [Article]

Levi, D. M., & Klein, S. A. (1990). The role of separation and eccentricity in encoding position. *Vision Research, 30,* 557–585.

Levi, D. M., & Tripathy, S. P. (1996). Localization of a peripheral patch: The role of blur and spatial frequency. *Vision Research, 36,* 3785–3803.

Lu, Z. L., & Dosher, B. A. (1999). Characterizing human perceptual inefficiencies with equivalent internal noise. *Journal of the Optical Society of America A, 16,* 764–778.

Manjeshwar, R. M., & Wilson, D. L. (2001). Effect of inherent location uncertainty on detection of stationary targets in noisy image sequences. *Journal of the Optical Society of America A, 18,* 78–85.

Michel, M. M., & Geisler, W. S. (2009). Gaze contingent displays: Analysis of saccadic plasticity in visual search. *Society for Information Display Technical Digest, 40,* 911–914.

Myers, K. J., Barrett, H. H., Borgstrom, M. C., Patton, D. D., & Seeley, G. W. (1985). Effect of noise correlation on detectability of disk signals in medical imaging. *Journal of the Optical Society of America A, 2,* 1752–1759.

Najemnik, J., & Geisler, W. S. (2005). Optimal eye movement strategies in visual search. *Nature, 434,* 387–391.

Palmer, J. (1994). Set-size effects in visual search: The effect of attention is independent of the stimulus for simple tasks. *Vision Research, 34,* 1703–1721.

Palmer, J., Ames, C. T., & Lindsey, D. T. (1993). Measuring the effect of attention on simple visual search. *Perception, 19,* 108–1130.

Palmer, J., Verghese, P., & Pavel, M. (2000). The psychophysics of visual search. *Vision Research, 40,* 1227–1268.

Peli, E., Yang, J., & Goldstein, R. (1991). Image invariance with changes in size: The role of peripheral contrast thresholds. *Journal of the Optical Society of America A, 8,* 1762–1774.

Pelli, D. G. (1981). *Effects of visual noise*. PhD thesis, Cambridge University.

Pelli, D. G. (1985). Uncertainty explains many aspects of visual contrast detection and discrimination. *Journal of the Optical Society of America A, 2,* 1508–1532.

Pelli, D. G. (2008). Crowding: A cortical constraint on object recognition. *Current Opinion in Neurobiology, 18,* 445–451.

Pelli, D. G., Palomares, M., & Majaj, N. J. (2004). Crowding is unlike ordinary masking: Distinguishing feature integration from detection. *Journal of Vision, 4*(12):12, 1136–1169, http://www.journalofvision.org/content/4/12/12, doi:10.1167/4.12.12. [PubMed] [Article]

Pelli, D. G., Tillman, K. A., Freeman, J., Su, M., Berger, T. D., Majaj, N. J., et al. (2007). Crowding and eccentricity determine reading rate. *Journal of Vision,*

7(2):20, 1–36, http://www.journalofvision.org/content/7/2/20, doi:10.1167/7.2.20. [PubMed] [Article]

Pelli, D. G., & Zhang, L. (1991). Accurate control of contrast on microcomputer displays. *Vision Research, 31,* 1337–1350.

Peterson, W., Birdsall, T., & Fox, W. (1954). The theory of signal detectability. *IEEE Transactions on Information Theory, 4,* 171–1212.

Petrov, Y., & Popple, A. V. (2007). Crowding is directed to the fovea and preserves only feature contrast. *Journal of Vision, 7*(2):8, 1–9, http://www.journalofvision.org/content/7/2/8, doi:10.1167/7.2.8. [PubMed] [Article]

Shaw, M. (1982). Attending to multiple sources of information: I. The integration of information in decision making. *Cognitive Psychology, 14,* 353–409.

Shiffrin, R. M., McKay, D. P., & Shaffer, W. O. (1976). Attending to forty-nine spatial positions at once. *Journal of Experimental Psychology: Human Perception and Performance, 2,* 14–22.

Sullivan, G. D., Oatley, K., & Sutherland, N. S. (1972). Vernier acuity as affected by target length and separation. *Perception & Psychophysics, 12,* 438–444.

Swensson, R. G., & Judy, P. F. (1981). Detection of noisy visual targets: Models for the effects of spatial uncertainty and signal-to-noise ratio. *Perception & Psychophysics, 29,* 521–534.

Tanner, W. (1961). Physiological implications of psychophysical data. *Annals of the New York Academy of Sciences, 89,* 752–765.

Toet, A., & Levi, D. M. (1992). The two-dimensional shape of spatial interaction zones in the parafovea. *Vision Research, 32,* 1349–1357.

Watt, R. J. (1984). Towards a general theory of the visual acuities for shape and spatial arrangement. *Vision Research, 24,* 1377–1386.

Watt, R. J., & Morgan, M. J. (1984). Spatial filters and the localization of luminance changes in human vision. *Vision Research, 24,* 1387–1397.

Werner, S., & Diedrichsen, J. (2002). The time course of spatial memory distortions. *Memory & Cognition, 30,* 718–730.

Westheimer, G. (1982). The spatial grain of the perifoveal visual field. *Vision Research, 22,* 157–162.

White, J., Levi, D., & Aitsebaomo, A. (1992). Spatial localization without visual references. *Vision Research, 32,* 513–526.

Wilson, H. R. (1986). Responses of spatial mechanisms can explain hyperacuity. *Vision Research, 26,* 453–469.

Yap, Y. L., Levi, D. M., & Klein, S. A. (1987). Peripheral hyperacuity: Isoeccentric bisection is better than radial bisection. *Journal of the Optical Society of America A, Optics and Image Science, 4,* 1562–1567.

Zhang, Y., Pham, B. T., & Eckstein, M. P. (2006). The effect of nonlinear human visual system components on performance of a channelized Hotelling observer in structured backgrounds. *IEEE Transactions on Medical Imaging, 25,* 1348–1362.